Identify Finger Rotation Angles With ArUco Markers and Action Cameras

Yuan, T.; Song, Y.; Kraan, G.A.; Goossens, R.H.M.

DOI
10.1115/1.4053409

Publication date
2022

Document Version
Final published version

Published in
Journal of Computing and Information Science in Engineering

Identify Finger Rotation Angles With ArUco Markers and Action Cameras

Tianyun Yuan[1]
Delft University of Technology,
Landbergstraat 15,
2628 CE Delft, The Netherlands
e-mail: t.yuan@tudelft.nl

Yu (Wolf) Song
Delft University of Technology,
Landbergstraat 15,
2628 CE Delft, The Netherlands
e-mail: Y.Song@tudelft.nl

Gerald A. Kraan
Reinier de Graaf Hospital,
Reinier de Graafweg 5,
2625 AD Delft, The Netherlands
e-mail: g.kraan@rhoc.nl

Richard H. M. Goossens
Delft University of Technology,
Landbergstraat 15,
2628 CE Delft, The Netherlands
e-mail: R.H.M.Goossens@tudelft.nl

Measuring the motions of human hand joints is often a challenge due to the high number of degrees-of-freedom. In this study, we proposed a hand tracking system utilizing action cameras and ArUco markers to continuously measure the rotation angles of hand joints during motion. Three methods were developed to estimate the joint rotation angles. The pos-based method transforms marker positions to a reference coordinate system and extracts a hand skeleton to identify the rotation angles. Similarly, the orient-x-based method calculates the rotation angles from the transformed x-orientations of the detected markers in the reference coordinate system. In contrast, the orient-mat-based method first identifies the rotation angles in each camera coordinate system using the detected orientations and then synthesizes the results regarding each joint. Experiment results indicated that the repeatability errors with one camera regarding different marker sizes were around 2.64–27.56 deg and 0.60–2.36 deg using the marker positions and orientations, respectively. With multiple cameras employed, the joint rotation angles measured by using the three methods were compared with that measured by a goniometer. Comparison results indicated that the results of using the orient-mat-based method are more stable and efficient and can describe more types of movements. The effectiveness of this method was further verified by capturing hand movements of several participants. Therefore, it is recommended for measuring joint rotation angles in practical setups. [DOI: 10.1115/1.4053409]

Keywords: hand tracking, hand kinematics, finger rotation angle

1 Introduction

The human hand is a marvel of dexterity, which is enabled by 27 bones and 19 joints (excluding the radiocarpal joint) [1,2]. Literature studies indicated that simplified full-hand kinematic skeletons often have as many as 18–27 degree-of-freedoms (DOFs) [3–5], which often pose challenges to hand kinematic studies, e.g., scanning and tracking the hand motion in various scenarios [6,7]. However, tracking hand movements to improve the understanding of hand kinematic is essential in the design of human–computer interaction [8,9], robotic grippers [10], and medical and rehabilitation devices [11,12].

Among all methods to measure the joint rotation angles, an (electro-) goniometer is the most classical way in clinical practice [13]. However, the quality of the results strongly depends on the skill and the experience of the user. Large interobserver and intraobserver variations are inevitable [13,14], e.g., the intraobserver variation might reach 4–10 deg [15,16]. Besides, it is challenging for both the participant(s) and the operator(s) when measuring multiple finger joints using a goniometer.

Advancements in technology enable measuring the finger joint rotations in a dynamic setup, where the sensor-based and vision-based approaches are typical examples [17–20]. In applications using inertial measurement units (IMUs), the sensor modules are often placed at the dorsal side of the hand for estimating joint rotations using the data from accelerometers and gyroscopes (and magnetometers if available) [21]. The repeatability errors of those systems were reported in the range of 2–10 deg [21–24]. However, professional 6 DOF IMUs can achieve an orientation accuracy of 0.5 deg (root-mean-square-errors) [25]. The flex sensor is another type of sensor employed to measure joint rotation angles. It is thinner and less intrusive with a repeatability error around 4–10 deg [26,27]. Some commercial data gloves using flex sensors reported a repeatability error within 2 deg [28,29]. However, the movements of the hand and the glove are not always the same due to the fit of the glove. Besides, cables are often required to transmit data and supply power, which further limit the hand movements in performing some daily activities, such as precise manipulations.

On the contrary, the vision-based approaches enable more free movements of hands as the sensors (e.g., cameras) have noncontact with the hand. Typical examples of these approaches are marker-based systems, which capture hand movements by tracking the positions of the optical markers/reflectors attached to fingers [30,31]. In the past decade, advancements in electronics and computer sciences enable more affordable solutions with cameras and fiducial markers, e.g., ArUco marker [32]. One ArUco marker can provide both the spatial position and orientation of the marker based on a 2D image projection. A recent study [33] on measuring the rotation angle of a robot finger indicated that the repeatability error of using ArUco marker was comparable to that of using IMU modules. In addition to the marker-based systems, many marker-less hand tracking systems, which utilized large databases and machine learning algorithms, were developed recently [34–36]. They can achieve around 10–50 mm accuracy in hand pose estimation. However, the effectiveness of such systems highly depends on the quality of the associated database captured by other motion capturing system(s) [35].

In this study, we present a low-cost vision-based tracking system to continuously measure the rotation angles of all finger joints during different types of movements. The aim of the research is to find the best practice of the setup of the system and the data processing methods. The remainder of this article is arranged as follows. In Sec. 2, the hardware of the proposed system is introduced. Section 3 elaborates the data processing process with the focus on identifying the orientation of the markers. In Sec. 4, we present details of the proposed three methods. Then, the repeatability errors and the measurable range of one camera are reported

[1]Corresponding author.

Contributed by the Computers and Information Division of ASME for publication in the Journal of Computing and Information Science in Engineering. Manuscript received August 21, 2021; final manuscript received December 24, 2021; published online February 7, 2022. Assoc. Editor: Paul Witherell.

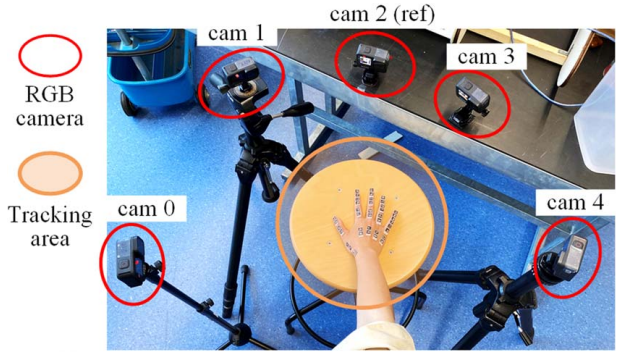

Fig. 1 The setup of the tracking system

Table 1 The settings of the cameras for video recording

Resolution	5 K (5120 × 2880 pixels)	Frames per second	30 fps
Field of view	Wide	Bit rate	High
Shutter speed	1/60	Sharpness	Medium
ISO min	100	ISO max	400

in Sec. 5, followed by the results of the experiments with a wooden hand and the experiments on tracking hand movements. Section 6 discusses the results and the use of the proposed system. Finally, a short conclusion is drawn.

2 The Tracking System

The proposed system utilizes five cameras (Brand: GoPro Hero 9) to locate and track ArUco markers as shown in Fig. 1. Forty ArUco markers [32] are sticked at the dorsal side of a right hand of the subject. Centered on the hand to be tracked, cameras are positioned toward the hand along a virtual semicircle with a diameter of approximately 500 mm. Instead of using static images, we utilize 30 fps 5 K videos to record hand movements. Detailed settings of the videos are listed in Table 1. To minimize possible errors introduced by lens distortion, all cameras are calibrated individually with a 12 × 9 checkerboard before data acquisition. In the calibration process, we position the board at different distances and inclination angles regarding the image plane of the camera to cover the envelope of the field of view of the camera.

The ArUco markers are generated using the 4 × 4 ArUco dictionary. The markers are printed on 300-g thick papers using an inkjet printer to promise a flat surface during the movements and avoid reflections. The approximate size of each marker is 9 × 9 mm, and this size is selected through several pilots with different participants and the anthropometry database [37]. The forty markers are grouped into 20 pairs following a linear alignment strategy [4], where each pair of markers represents a corresponding segment of the skeleton model in Fig. 2(*c*). Here, the *x*-axes of the markers are strategically placed toward the distal direction of the hand, and hence, markers on each finger are approximately aligned along the axis of the finger as shown in Figs. 2(*a*) and 2(*b*). With the positions and orientations of detected markers, rotation angles between finger segments can be calculated. We extract the flexion—extension (flx-ext) (Fig. 2(*b*)) angles of all highlighted joints in Fig. 2(*c*) and the radial—ulnar (rad-uln) angles (Fig. 2(*a*)) of the joints with solid circles in Fig. 2(*c*). Here, although the MPJ for thumb has two DOFs in reality, only the flx-ext movement is presented in the results.

3 Data Processing

3.1 The Workflow. Figure 3 presents the workflow of data processing, along with the usage of the positions and orientations of the detected markers. The videos from different cameras are synchronized first based on their audio streams. Then using OpenCV, the ArUco library, and the adjusted marker size, the positions and orientations of the detected markers in all frames of each video are extracted regarding the corresponding camera coordinate system (CCS). By intercalibration, all camera coordinates are associated with a reference coordinate system (RCS) and identify the correct orientation in two possible solutions of each marker. After this, the joint rotation angles are calculated using the three proposed methods. The *pos-based* and *orient-x-based* methods first gather all detected marker positions and orientations of a frame in the RCS and calculate the angles between two corresponding spatial vectors of a joint. Differently, the *orient-mat-based* method first calculates the Euler angles with the detected orientations in each CCS and then synthetizes all angles identified in different videos regarding each joint.

3.2 Marker Size Estimation and Intercalibration Among Cameras. Before each experiment, extra videos of an 8 × 10 ChArUco board are taken for marker size estimation and intercalibration. The board includes markers of the same size as the markers used for hand tracking, and the board is moved to fill the envelope

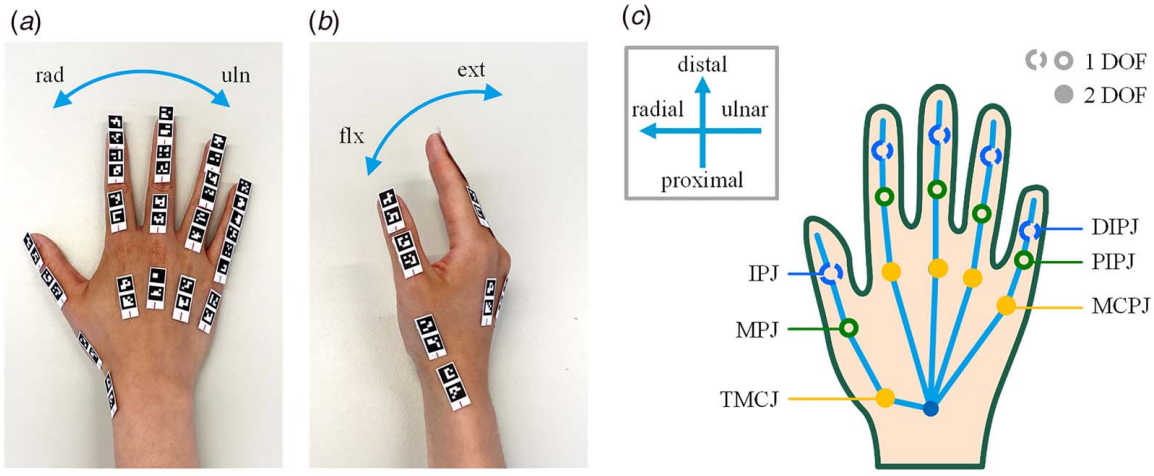

Fig. 2 Place the markers on the hand: (*a*) top view, (*b*) side view, and (*c*) the skeletal model of the right hand. Rad, radial direction; uln, ulnar direction; flx, flexion; ext, extension; IPJ, interphalangeal joint; MPJ, metacarpophalangeal joint; TMCJ, basal carpometacarpal joint; DIPJ, distal interphalangeal joint; PIPJ, proximal interphalangeal joint; MCPJ, metacarpophalangeal joint.

of the tracking with different inclination angles. After video synchronization, the positions of the markers on the board are then employed to identify marker sizes for each camera and identify the transformation matrices among cameras.

The marker size, defined as the width of the square pattern, is essential in the estimation of marker positions. Since the intrinsic properties vary among cameras, a distance measured in reality may be different from the distance measured in the CCS. Thus, the distances between two horizontally adjacent markers on the board are measured by a Vernier caliper and computed based on the marker positions extracted from the video of each camera. Then, the marker size can be retrieved when the mean values of these two types of distance are almost the same, and this process is repeated for all cameras. Based on the identified marker sizes, the positions of the markers are computed for intercalibration and further processes.

To identify the transformation matrix between a camera and the RCS, the detected marker positions $p_{i,j}^k$ is compared with the corresponding marker positions $p_{i,j=RCS}^k$ (if any). In our setup, *cam 2* in Fig. 1 is selected as the reference camera, and its coordinate system is then the RCS. The transformation matrix from the jth CCS (including translation T_j and rotation parts R_j) to the RCS can be found by solving Eq. 1 using the singular value decomposition:

$$\text{argmin} \sum ||(R_j \cdot p_{i,j}^k - T_j) - p_{i,j=RCS}^k|| \tag{1}$$

where $p_{i,j}^k$ is the positions of the marker with index i at the kth synchronized frame in the jth CCS; T_j and R_j are the translation and rotation part of the transformation matrix, respectively. By using the transformation matrix, the transformed position $P_{i,j}^k$ in the RCS of position $p_{i,j}^k$ is calculated using Eq. 2:

$$P_{i,j}^k = R_j \cdot p_{i,j}^k - T_j \tag{2}$$

3.3 Marker Orientation Selection. By analyzing the images of the videos frame by frame, spatial orientations of the detected markers are extracted along with positions. In the process of identifying the orientations of detected markers, there might have ambiguous results due to the optical illusions [38]. In short, there are two possible solutions in the estimation of a 3D cube from a 2D quadrilateral. Although both can be obtained using the PnP solver, only one of them is the desired solution. This leads to problems in extracting the desired orientations, and it is especially difficult when the optical axis of the camera is close to the normal direction of the marker(s). Before the involvement of manual selections, we utilize the rotation part of the transformation matrices R_j identified in Eq. 1 and two algorithms, Algorithm 1 and 2, to assist the selection procedure. The algorithms are explained with a simplified example shown in Fig. 4, where the x-axis stands for time frame, and the y-axis is the number of cameras that detect a marker $i = i_0$ at each frame $k = 0..k_0..l$.

Algorithm 1

Input: Intercalibration matrix T_j; the possible z-axis orientation $\{oz_{i,j}^{k,u},\ k = 0, 1, \ldots, l,\ u = 0\ or\ 1,\ i = 0, 1, \ldots, m,\ j = 0, 1, \ldots, n\}$; $oz_{i,j}^{k,u} = NA$ if marker was not detected

Output: $K1$, frames with u selected; $K2$, frames with u undecided; $U = \{\ u_{i,j}^k |\ u = 0\ or\ 1,\ for\ any\ i, j, k\}$, set of selected u

Process:

For any $i,\ j,\ k,\ u{:}OZ_{i,j}^{k,u} = R_j \cdot oz_{i,j}^{k,u}$

Loop $k,\ i,\ j$:

$k_0 = k,\ i_0 = i,\ j_o = j$

find $\{j|\ OZ_{i=i_0,j=j_0}^{k=k_0,u} \neq NA\}$ and build set $zj = \{j\}$

If *length* $(zj) \geq 2$:

$u_{i=i_0,j=j_0}^{k=k_0} = \text{argmin}_{u=0,1,\ j\in(zj)}\{\arccos(OZ_{i=i_0,j=j_0}^{k=k_0,u}, OZ_{i=i_0,j\neq j_0}^{k=k_0,u})\}$

$K1_{i,j} = \{k|\text{where } u \text{ is selected}\}$

$K2_{i,j} = \{\ k|\ \text{where } oz_{i,j}^{k,u} \neq NA\ and\ k \notin K1_{i,j}\}$

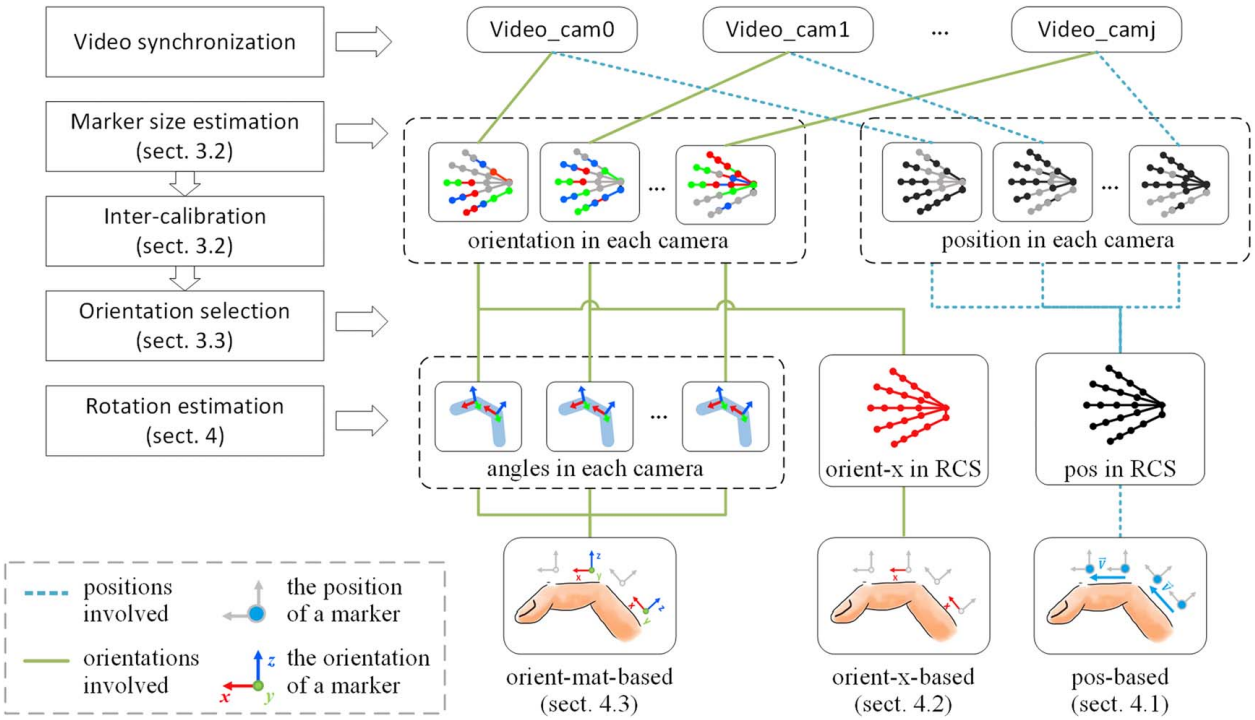

Fig. 3 The workflow for data processing and the usage of marker positions and orientations

Algorithm 2

Input: $\{oz_{i,j}^{k,u},\ k=0,1,\ldots,l,\ u=0\ or\ 1,\ i=0,1,\ldots,m,\ j=0,1,\ldots,n\}$
$(oz_{i,j}^{k,u}=NA$ if not found);
$K1$, frames with u selected; $K2$, frames with u undecided;
$U=\{\ u_{i,j}^{k}|\ u=0\ or\ 1,\ for\ any\ i,j,k\}$; $\delta=$ frame threshold
Output: $U=\{\ u_{i,j}^{k}|\ u=0\ or\ 1,\ for\ any\ i,j,k\}$
Process:

If $K2_{i=i_0,j=j_0} \notin \varnothing$:
  Loop $i,\ j$:
    $i_0=i,\ j_o=j$
    For each $k_0 \in K2_{i=i_0,\ j=j_0}$)
      $K_{i=i_0,j=j_0}^{nearby}=[\max(0,\ k_0-\delta),\ \min(k_0+\delta,\ l)]$
      If $refK_{i=i_0,j=j_0}^{k=k_0}=(K_{i=i_0,j=j_0}^{nearby} \cap K1_{i=i_0,j=j_0}) \neq \varnothing$:
    $u_{i=i_0,j=j_0}^{k=k_0}=\text{argmin}_{u=0,1,j=j_0}\{\arccos(OZ_{i=i_0,j=j_0}^{k=k_0,u}, OZ_{i=i_0,j=j_0}^{k\in refK,u\in U})\}$
    Add $k=k_0$ to $K1$ where $i=i_0,\ j=j_0$
    Delete $k=k_0$ from $K2$ where $i=i_0,\ j=j_0$
Else manual involvement

Algorithm 1 uses the information in the synchronized frame gathered by any two cameras to help the selection. First, all the possible solutions of z-axis orientations $oz_{i,j}^{k,u}$ are transformed to RCS as $OZ_{i,j}^{k,u}=R_j \cdot oz_{i,j}^{k,u}$. Here, i, j, and k are the same as Eq. 1 and $u=0$ *or* 1, which implies the two possible solutions. For any aligned frame, when a marker is visible by multiple cameras from different viewing angles, two possible solutions $oz_{i,j}^{k,u=0}$ and $oz_{i,j}^{k,u=1}$ of the ith marker in the jth camera at the frame k are compared with that of other cameras and form $4(n-1)$ (pairs) possible combinations. Here, n is the number of cameras that detect this marker at the synchronized frame. In practices, n is often 2 or 3 in the proposed setup. Among these different combinations, the solution of the jth camera that leads to the least angular difference among the possible combinations is considered as the desired solutions. With Algorithm 1, the solutions of a marker detected by multiple cameras, i.e., the solid areas in Fig. 4 and $K1$ in the algorithms are determined. The set U, which notes the selected u value, is updated. $K2$, which is the output of Algorithm 1, retains the undetermined frames, and the marker of these frames are visible by only one camera, such as the areas with patterns in Fig. 4.

Based on the information of each camera itself, Algorithm 2 is applied to select the desired solution for $K2$ along the time frame based on the decision of $K1$. The solutions are decided by comparing the two possible z-axis orientations of a marker in any undecided frames in $K2$ with the determined z-axis orientation of this marker in the nearby frames in $K1$. Similar to the Algorithm 1, the solution with the least angular difference is taken as the desired solution, as the similar motion status is expected within a threshold of 15 frames (approximately 0.5 s) regarding the practical movement speed. By iterating this procedure for all undetermined frames sets $K1$, $K2$, and U are updated automatically. Then, the solutions of frames as the solid areas and the areas with diagonal stripes in Fig. 4 are also decided. However, manual effort is still required for situations as the area with horizontal stripes in Fig. 4, where no extra information can be compared neither with other cameras nor within a credible range of frames.

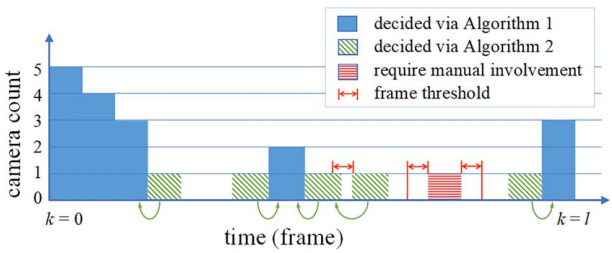

Fig. 4 An example of a marker $i=i_0$ detected by different number of cameras regarding consecutive frames

4 Estimation of Joint Rotation Angles

4.1 The Pos-Based Method. The *pos-based* method utilizes the positions of detected markers in synchronized frames of the videos from different cameras and transforms all camera coordinates to the *RCS*. Based on the transformed positions of each marker $P_{i,j}^{k}$, a simplified hand skeleton is constructed and the joint rotation angles regarding the initial position of the hand is calculated. Marker positions detected in each camera are transformed to the RCS and plotted in different types of markers in Fig. 5(*a*). The mean values of each corresponding markers, $\bar{P}_i^k=\sum_j P_{i,j}^k/n$ (n indicates the number of cameras that capture this marker) are used to construct a hand skeleton at the kth frame, as shown in Fig. 5(*b*). Then, a vector constructed by the two paired markers, $V_{seg}=\bar{P}_{dis}^k-\bar{P}_{pro}^k$, represents the corresponding finger segment, pointing from the proximal to the distal direction. The vectors of the third and fourth metacarpals, V_{m3} and V_{m4}, as highlighted in Fig. 5(*c*), are used to establish the coordinate system of the hand (CS_{hand}) [39] for determining the rotation direction, and the origin of CS_{hand} is the position of the proximal marker of the third metacarpal segment as shown in Fig. 5(*d*). The x_{axis} of CS_{hand} is the unit vector of V_{m3}, the z_{axis} is the unit vector of the cross product of V_{m4} and V_{m3}, and the y_{axis} is the unit vector of the cross product of z_{axis} and x_{axis}.

Based on the CS_{hand} and the found vectors of each finger segment $\{V_{seg},\ seg \in hand\ skeleton\}$, the flx-ext and rad-uln rotation angles can be calculated using Eq. 3. In the equation, the direction of the rotation angle is decided by comparing the cross vector of the two segments with a reference vector V_{ref}, which is the y_{axis} of CS_{hand} for flx-ext angles and the z_{axis} of CS_{hand} for rad-uln angles.

$$\theta = \text{signum}((V_{prx} \times V_{dis}) \cdot V_{ref}\ ) \arccos(V_{prx} \cdot V_{dis}) \tag{3}$$

4.2 The Orient-x-Based Method. The *orient-x-based* method estimates joint rotation angles based on the transformed x-axis orientation of the detected markers. Different from the *pos-based method*, this method directly applies the x-axis orientations of detected markers as the vector representing the finger segments, as illustrated in Fig. 6. In practice, we use the x-orientation of the proximal marker in the pair. Therefore, information of only half of the markers is needed.

Given $ox_{i,j}^k$, which is the x-axis orientation of the ith marker in the kth frame in the jth CCS, it is first transformed to the RCS by $OX_{i,j}^k=R_j \cdot ox_{i,j}^k$. The mean orientation $\overline{OX}_i^k=\sum_j OX_{i,j}^k/n$ is used

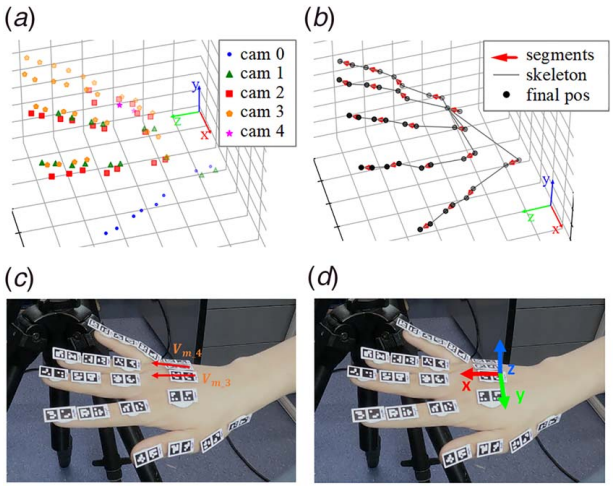

Fig. 5 The process of extracting hand skeleton ((*a*) marker positions and (*b*) skeleton) and (*c* and *d*) constructing the hand coordinate

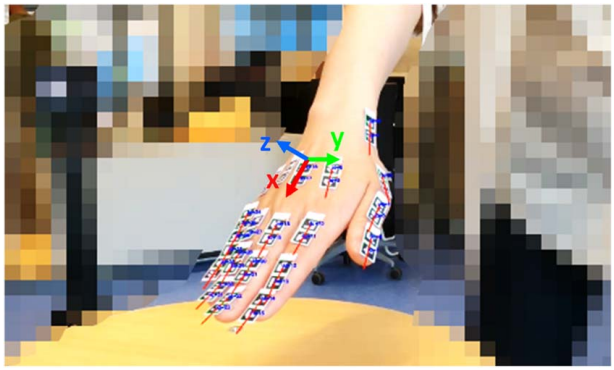

Fig. 6 *X*-axes of each finger segment and the hand coordinate

to calculate the rotations, where n is the number of cameras that detect this marker. Same as the *pos-based method*, the x-axis orientation of the third and fourth metacarpal is applied to construct the CS_{hand} as shown in Fig. 6. Afterward, the x-axis orientations of two adjacent finger segments are used to compute the rotation angles following Eq. 4. The rotation direction is decided by comparing the $V_{ref} = y_{axis}$ *of* CS_{hand} and $V_{ref} = z_{axis}$ *of* CS_{hand} for the flx-ext and the rad-uln angles, respectively.

$$\theta = \text{signum}((OX_{prx} \times OX_{dis}) \cdot V_{ref}) \arccos(OX_{prx} \cdot OX_{dis}) \quad (4)$$

4.3 The Orient-Mat-Based Method. Different from the *orient-x-based method*, the orientations of all three axes of detected markers are used in the *orient-mat-based method*. In practice, we adopt the orientation of the proximal marker in the pair to represent the orientation of the corresponding finger segment $om^k_{i,j}$, where i, j, and k are the same as Sec. 4.2. Figure 7 presents the $om^k_{i,j}$ of the markers at their positions. Here, the x_{axis} of the marker points from proximal to distal side, y_{axis} points from the ulnar to the radial side, and z_{axis} points from the palmar to the dorsal side.

Instead of transforming to the RCS, the orientations detected in each CCS are directly used to estimate the joint rotation angles. A rotation matrix R^m is identified between the orientations of two adjacent finger segments $om^k_{prx,j}$ and $om^k_{dis,j}$ as follows:

$$R^m = om^k_{dis,j}(om^k_{prx,j})^{-1} = \begin{bmatrix} a_{00} & a_{01} & a_{02} \\ a_{10} & a_{11} & a_{12} \\ a_{20} & a_{21} & a_{22} \end{bmatrix} \quad (5)$$

Based on Eq. 5 and the methods described in Refs. [40,41], Euler angles (β, γ, α) are calculated following Y-Z-X sequence as follows:

$$\beta = \arctan\frac{a_{02}}{a_{00}}, \quad \gamma = \arcsin(-a_{01}), \quad \alpha = \arctan\frac{a_{21}}{a_{11}} \quad (6)$$

where β, γ, and α correspond to the rotation of flx-ext, rad-uln, and self-rotation (pronation-supination) of the joint, respectively. Then, the final rotation angles of each joint are computed as the mean of the rotation angles of this joint identified by any cameras as $\{\alpha, \beta, \gamma\}^k_{\text{joint}} = \sum_j \{\alpha, \beta, \gamma, \}^k_{\text{joint},j})/n$, where n indicates the number of cameras that are able to identify the rotation angle of this joint.

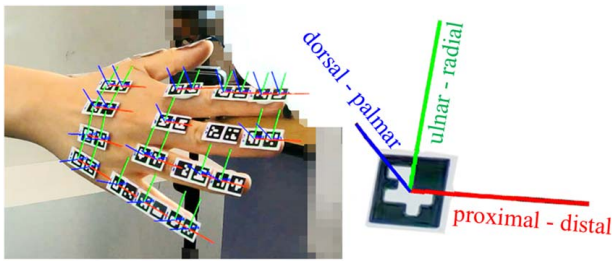

Fig. 7 The orientation of detected markers (x_{axis}: proximal-distal, y_{axis}: ulnar-radial, z_{axis}: dorsal-palmar)

Table 2 The distance/deviation of intercalibration

Camera	Registered points	Distance difference (*pos-based*), mean (±SD) (mm)	Angular difference (*orient-x-based*), mean (±SD) (deg)
Cam 0	22,958	3.91 (±13.07)	2.85 (±3.26)
Cam 1	63,016	3.98 (±4.36)	2.23 (±2.37)
Cam 2 (ref)	84,351	3.29 (±3.16)	2.40 (±2.46)
Cam 3	64,144	2.73 (±4.34)	1.76 (±2.15)
Cam 4	19,192	7.59 (±66.43)	2.18 (±5.18)

5 Experiments

This section first presents the calibration result of the proposed system, followed by the setups and the results of an experiment conducted on the platform of a milling machine. This experiment investigated the accuracy, the repeatability, and the measurable range using one camera. Then, five cameras were employed to track a wooden hand with fixed joints to study the difference between the measurement results of using a goniometer and using the three proposed methods. Finally, with the proposed system, the joint rotations of three participants in performing a continuous hand movement were analyzed.

5.1 Camera Calibration Results. An average of 153 images was used to identify the lens distortions of each camera, and the projection errors were about 0.088–0.102. Five cameras were adopted, and one of the cameras (*cam 2* in this study) was chosen as the reference. The mean values $\bar{P}^k_i$ and $\overline{OX}^k_i$ were calculated from the gathered information in the RCS, and they were compared with transformed positions $P^k_{i,j}$ and x-axis orientations $OX^k_{i,j}$ of each camera, respectively. The number of registrable points and the mean differences of these points and the orientations of markers are listed in Table 2.

5.2 Accuracy, Repeatability, and Measurable Range. To study the effectiveness of the proposed system, we designed an experiment to investigate the accuracy, repeatability, and measurable range of one camera. Three sets of markers were prepared, and each set included seven pairs of markers with different marker sizes. These sizes were measured using a Vernier Caliper. The three sets of markers were placed on a standard metal workpiece, which has three flat surfaces as shown in Fig. 8(*b*).

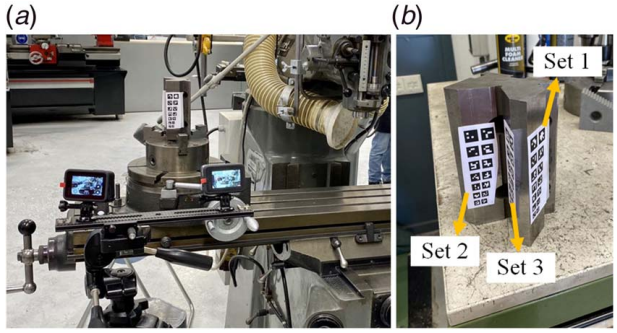

Fig. 8 Setup of the experiment: (*a*) the setup and (*b*) three sets of markers that glued to the workpiece

The dihedral angle between the surfaces with Set 2 and Set 3 was 90 deg. This workpiece was fixed on the rotary table of a milling machine, as shown in Fig. 8(*a*), and the rotary table can be moved along the platform in three directions. Two cameras (one was to assist orientation selection) were placed about 25–30 cm away from the machine to acquire video clips. Only *the pos-based* and *the orientation-x-based* methods were used, as the *orient-x-based* and the *orient-mat-based* methods utilize the same orientation information from one camera and the difference is mainly in processing such information among cameras.

The first part of the experiment investigated the repeatability when using videos of one camera. The marker Set 1 was set facing toward the cameras, and then the workpiece was translated in a 500 × 200 ×100 mm envelope along three axes, each three steps in the camera view, resulting in 27 positions. During the translation, we paused the movement for 10 s at each position. After extracting all marker positions and orientations, the *x*-axis orientation deviations of paired markers were calculated using the *pos-based* method and the *orient-x-based* method regarding the *x*-axis of the camera coordinate, respectively. Theoretically, the angle deviation of each point in these 10 s would be zero as both the cameras and the markers were fixed. However, the deviations varied among the marker sizes as shown in Fig. 9, which presents the absolute errors (in deg) regarding the seven marker sizes (horizontal axis in the figure). The results of using the *orient-x-based* method were more stable (mean = 2.51–2.99, STD = 0.60–1.13 deg) compared to the *pos-based* method (mean = 4.45 to 19.43, STD = 2.64–13.11 degrees), which was quite sensitive to the marker size and the errors of small markers were considerably large.

The second part evaluated the accuracy of the proposed system. The angles between Set 2 and Set 3 were measured in different positions and angles toward the cameras. Hence, the rotary table was moved to the left, medium, and right in the view of one camera along a 500 mm axis. At each position, the workpiece was rotated in a 10-deg step to create different inclination angles regarding the image plane of the camera. The measured angles between Set 2 and Set 3 were expected to be 90 deg. The mean angles measured using the *orient-x-based* method were between 90.20 and 92.92 deg (STD = 1.26–2.36 deg) regarding the marker sizes. In comparison, the mean angles estimated using the *pos-based* method deviated much more, even for the markers with size larger than 9 mm, as presented in Fig. 10.

The third part was to find the measurable range of a marker in the view of one camera, when the marker placed in difference inclination angles to the image plane of the camera. In this test, the rotary table was placed at the center of the camera view, and the workpiece (with marker Set 1) was continuously rotated 360 deg while being recorded. Angles between the *x*-axis of the CCS and the vectors of the seven marker pairs were computed using the *pos-based* and *orient-x-based* methods, respectively. The approximate ranges of

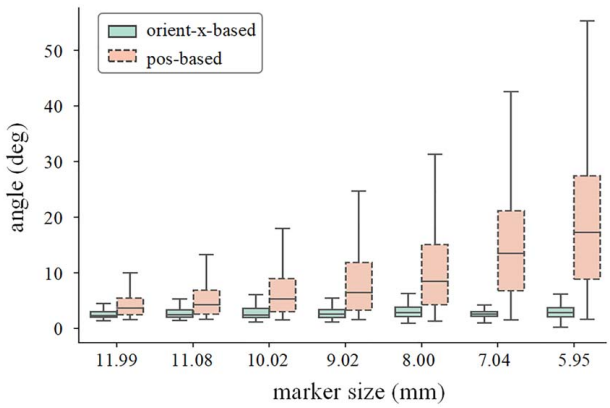

Fig. 9 The deviations regarding the size of markers for repeatability investigation

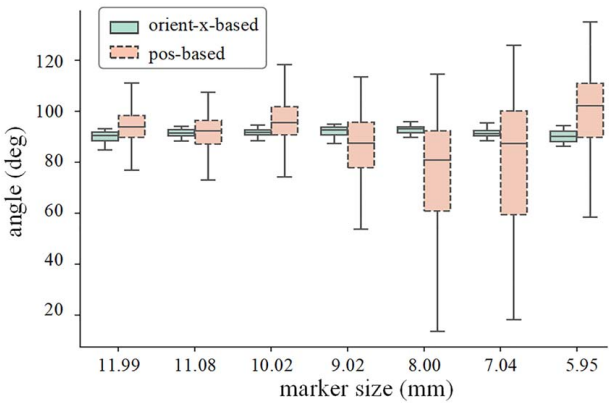

Fig. 10 The deviations regarding the sizes of markers for measuring the angles between Set 2 and Set 3

large markers were slightly larger than the ranges of small markers regardless the calculation methods, as presented in Fig. 11. Considering the results of both methods, the measurable range of a marker in the view of one camera was about 130–145 deg.

5.3 Rotation Measurement of a Wooden Hand. Before experiments with participants, a pilot study was conducted with a wooden hand model to measure joint rotations with a static pose. Two of the finger joints were fixed, and then a researcher held the bottom part of the model and moved it within the envelope of the tracking system. The angles estimated using three proposed methods were compared with the readings from a goniometer. The mean rotation angles of five measurements using the goniometer were around 32 and −15 deg for the two cases, representing the flexion and the extension, respectively. The results of the analysis using the three methods are plotted in Fig. 12, where the *x*-axes stand for the frames in the time domain and *y*-axes are the measured flx-ext angles at the corresponding frames. The mean values were 31.84 (±6.12) and −15.28 (±4.05) deg using the *pos-based* method; 32.05(±2.84) and −15.49(±0.58) deg with the *orient-x-based* method; and 32.58(±1.79) and −15.07(±0.58) using the *orient-mat-based* method. The mean rotation angles using three methods were close to the readings of the goniometer. However, the standard deviation with the *pos-based* method was larger than that of using the other two methods. In contrast, the rotations estimated using the *orient-x-based* and *orient-mat-based* methods were similar at each frame. Only a slight difference was observed, and part of the results of case (b) is zoomed-in at the right side of Fig. 12.

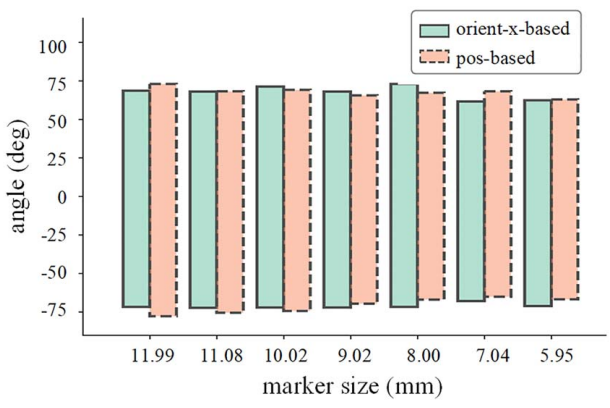

Fig. 11 Measurable ranges of one camera regarding different sizes of markers

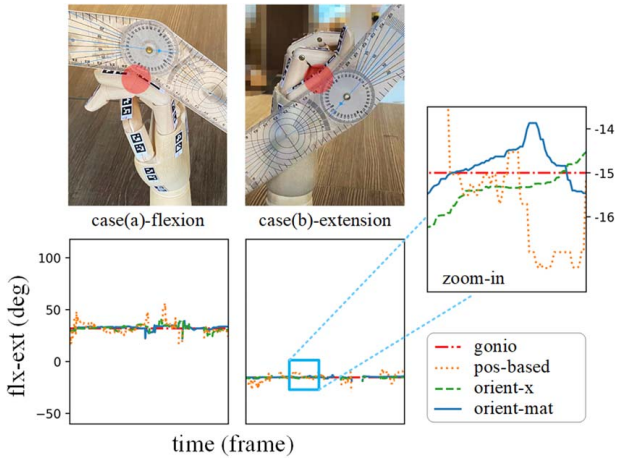

Fig. 12 The measured flx-ext angles of a wooden hand using the three methods

5.4 Rotation Measurement of Continuous Hand Movements. Hand movements of three volunteers were recorded and analyzed to evaluate effectiveness and efficiency of the proposed system and the rotation estimation methods. Participants were instructed to perform a series of movements, starting with the resting pose and then including abduction–adduction of all fingers and flexion-extension of all finger joints, as the screenshots in Fig. 13. The numbers of markers detected by each camera and the sum of them are plotted against the video frames in the figure. Most markers can be detected for the first two types of movements; however, the number of detected markers gradually became less during the flexing-extension of metacarpophalangeal joint (MCPJ). It was caused by the markers at the distal end of the fingers; when the participant bent those fingers towards the palm, those markers were invisible to either of the five cameras.

The joint rotation angles regarding to the resting pose (the initial frame) were calculated using the three methods. The measured rotation of the movement performed by one participant is highlighted in Fig. 14, where the five columns stand for the five fingers from thumb to pinky finger, and each row is in accordance with the flx-ext or the rad-uln rotation angles of the joints highlighted in Fig. 2(*c*). In each subfigure, the *x*-axis presents time frames and the *y*-axis presents the rotation angles in degrees, where the flexion rotation and the radial deviation are in positive values. Measurement results using the *pos-based*, the *orient-x-based*, and the *orient-mat-based* are presented in dotted, dashed, and solid lines, respectively. Comparing the three types of lines, the measured angles using the three methods are mostly comparable, but the abrupt deviation is observed when using the *pos-based* method. Also, large differences are identified when comparing the angles calculated using *the orient-mat-based method* to the results of using other two methods, as the gray areas highlighted in Fig. 14. These areas are all related to the joints with multiple DOFs, such as the MPJ and the basal carpometacarpal joint (TMCJ) for the thumb and the MCPJ for the other fingers. Conjectures regarding the differences will be detailed in Sec. 6.2.

By using the *orient-mat-based* method, we invited more participants to perform the same set of movements. Figure 15, which shares the same figure structure as Fig. 14, presents the results of three participants with hand size around P10, P60, and P40 (based on Ref. [37]). The trends of the three lines are different as though they performed the same actions, but with different motion speeds and motion ranges.

6 Discussion

6.1 Comparison Among the Three Methods. This study proposed a hand tracking system that utilized five RGB action cameras and ArUco markers to track hand movement and estimate joint rotation angles. On the basis of acquired positions and orientations of the markers, we measured finger joint rotations with three methods: the *pos-based*, the *orient-x-based*, and the *orient-mat-based* methods. Comparing the three methods, the latter two have an obvious advantage as they only need half of the number of markers required by using the *pos-based* method. Other benefits and drawbacks of using each of the proposed three methods are summarized in Table 3.

The experiment with the milling machine and the rotary table suggested that the repeatability errors of one camera were about 2.64–27.56 deg using marker positions and 0.60–2.36 deg using detected orientations. The results of using positions are less

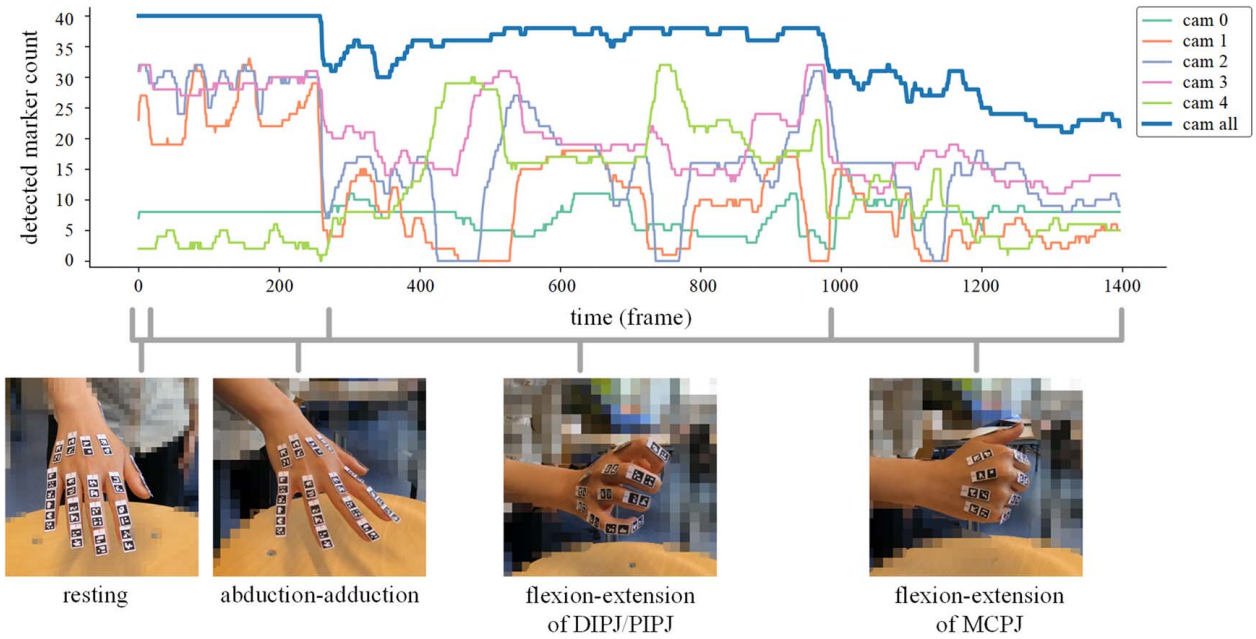

Fig. 13 The total number of the detected markers corresponding to the movement

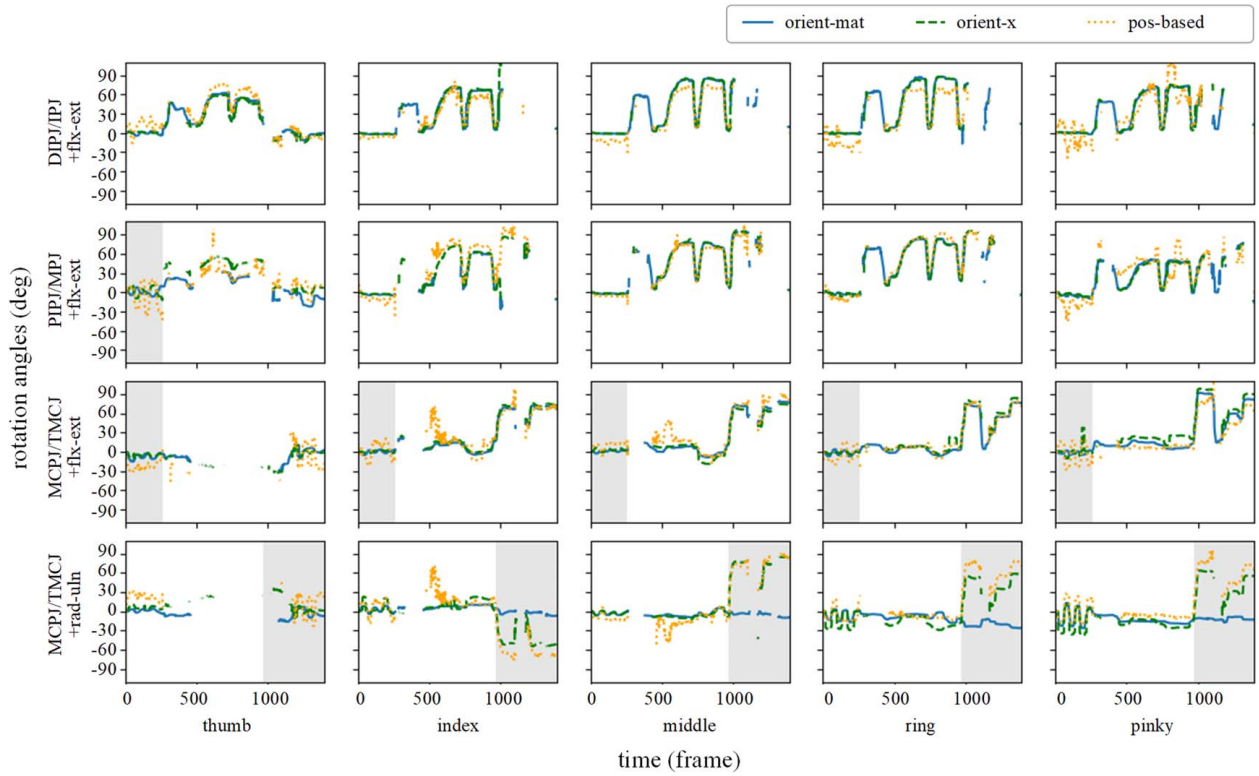

Fig. 14 Rotation anagles of each finger joints regarding time in frames

competitive compared with other tracking systems [21–24,27,28], but the results of using orientations are acceptable as it was less than 5 deg, which is a threshold in the evaluation of a tracking system [30] and in the studies of gait [42].

Considering the results of all the experiments, using the *pos-based* method often resulted in larger deviations than using other two methods. There are three conjectures, and two of them relate to the processes of estimating the marker sizes and intercalibration among cameras. The estimation of the marker size is critical to extract the correct marker positions, and small errors may introduce large deviations to the follow-up steps, e.g., intercalibration, and hand skeleton construction. On the contrary, the rotation estimation using the *orient-mat-based* method is independent of the marker size estimation and intercalibration. Another conjecture is the

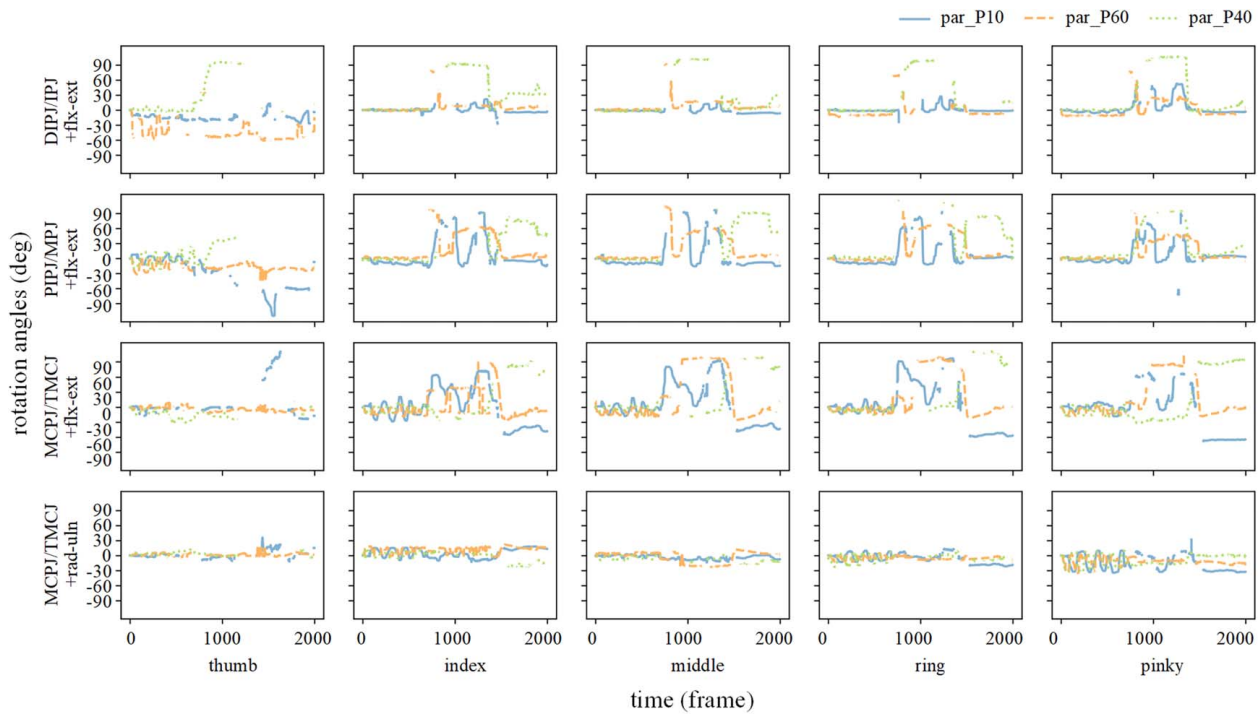

Fig. 15 Detected rotation angles of hand movements of different participants using the *orient-mat-based* method

Table 3 A comparison of using the proposed three methods

	Pos-based	*Orient-x-based*	*Orient-mat-based*
Data processing	– 40 markers – Requires marker size estimation – May have abbe error	+ Less markers (20) + Independent from marker size estimation /	+ Less markers (20) + Independent from marker size estimation /
Rotation estimation	/ + Information of the full skeleton – Requires a CS_{hand} + Is comparable to traditional measurements – One DOF rotation	– May need manual involvement + Information of the full skeleton – Requires a CS_{hand} + Is comparable to traditional measurements – One DOF rotation	– May need manual involvement – Measurable range of one camera + No need of a CS_{hand} – May be different to the traditional measurements + Can be applied to more scenarios

Note: "/" means do not apply.

abbe error. The length and breadth of finger segments limit the marker size and the distance between the paired markers, and thus, any errors in the position estimation could introduce large angular deviations.

6.2 Differences of the Rotation Estimation. The angles estimated using the three methods are similar in most cases as present in Fig. 14. However, differences are found in the gray area in Fig. 14, where the angles estimated using the *orient-mat-based* method are distinct from the angles extracted by the other two methods. Also in these areas, the absolute values of the angles calculated using the *orient-x-based* and the *pos-based* methods are equal to the absolute angles of the corresponding frames in another type of the movement (e.g., the absolute rad-uln angles of MCPJ/TMCJ after frame 1000 are the same as the absolute flx-ext angles of these joints). The rotation angles calculated by the *pos-based* and the *orient-x-based* methods are the angles between two corresponding vectors in 3D, while the rotation angles estimated using the *orient-mat-based* method are the Euler angles; these two types of angles are different mathematically. A previous article [43] discussed that only using vectors to estimate three-dimensional joint rotations can lead to errors because this calculation method relies on the assumption that the joints only have one DOF, which is not always true for all finger joints. This can be proved by the fact that the gray areas always occur with the joints with multiple DOFs, e.g., MCPJ, TMCJ, and MPJ. Although using the vectors to estimate rotations is theoretically following the same strategy of measuring the rotations with goniometers, which measures the joint rotation by placing the two sides of the meters along with two finger segments, respectively [44], it is unable to automatically classify the flx-ext rotation and rad-uln deviation into the correct movement type. Then, the estimated result includes the rotations caused by both flexion-extension and radial-ulnar deviation, e.g., thumb opposition. On the contrary, using the *orient-mat-based* method can still be applied in this case, as it extracts Euler angles of the

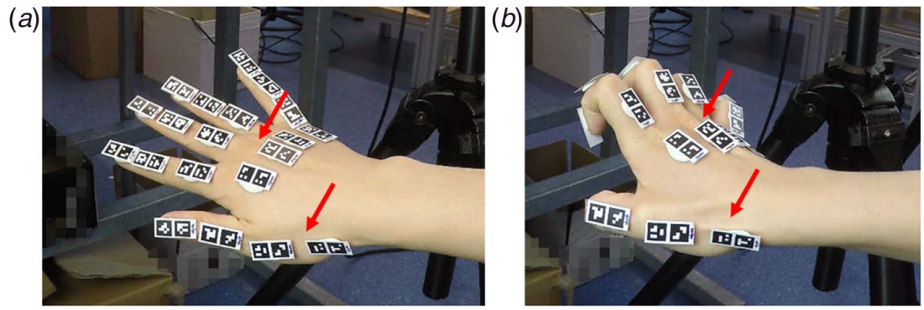

Fig. 16 Screenshots of the videos: (*a*) without and (*b*) with extensor digitorum tendons deformation

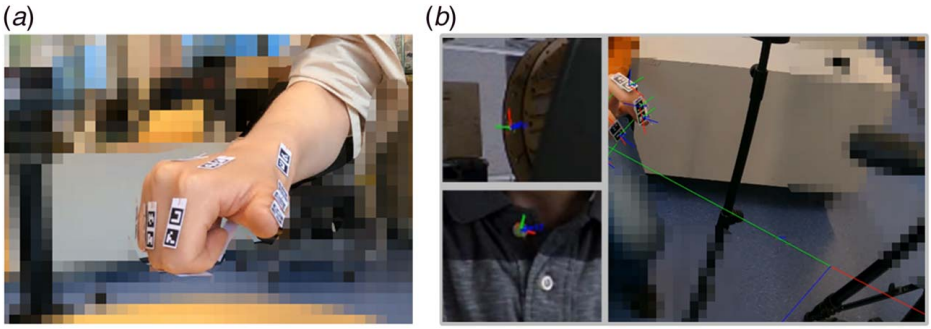

Fig. 17 Screenshot of the video: (*a*) the occlusion situation when markers on the distal segments were fully covered and (*b*) noise in the background and the fault in the detection of markers

rotations of three axes to classify three types of movements: flexion-extension, radial-ulnar deviation, and self-rotation. Thus, we suggest using the Euler angles for rotation estimation.

6.3 Limitation. In the experiments with participants, it was observed that markers rotated along the distal-proximal axis as connective tissues cause the deformation as presented in Fig. 16. This can introduce measurement error, especially for the self-rotation (pronation-supination). Theoretically, this has no/less influence on using the *pos-based* and the *orient-x-based* methods, and the self-rotation angles can be calculated by only using the *orient-mat-based* method. A better placement strategy will be explored to reduce such effects.

The proposed system successfully measured joint rotation angles continuously using the RGB cameras and ArUco markers, but the two issues of using a vision-based system still exist: occlusion and the noise of the environment [45]. For instance, for the first posture in Fig. 7(*a*), markers representing the distal phalanges are fully covered by the palm and were invisible by any of the cameras. Thus, information on this part was missing. Another example was the scenario shown in Fig. 17(*b*), and background noise confused the marker detection algorithm. Extra lighting was introduced to improve the detection results, but misdetection was still observed especially for markers with simple patterns, and light reflections on the markers may also led to the loss of the detection. For the latter issue, we printed the markers with an inkjet printer to minimize the reflection. The influence of marker pattern complexity will also be studied in the future.

7 Conclusion

In this article, we proposed a low-cost camera system to measure finger joint rotation angles using ArUco markers. Three methods, namely, the *pos-based*, the *orient-x-based*, and the *orient-mat-based* methods, were implemented to extract the rotation angles. The first two methods calculate the joint rotations as the angles between two corresponding vectors in the RCS. For the third method, the joint rotations are identified first as the Euler angles between the orientations of two bone segments in the coordinate system of one camera, and then the results of all camera are synthesized regarding each joint. Experiment results with one camera suggested that using the marker orientation was more stable as the repeatability error was comparable with previous studies using motion capture systems, sensor-based devices, or goniometers. In the use of multiple cameras, the *orient-mat-based* method outperformed the other two methods regarding both efficiency and reliability, as it is independent of the results of marker size estimation and intercalibration. Also, this method can be applied to more practical scenarios as it can describe the joint rotations in a more appropriate manner. Considering the quality of the results and efficiency of the process, we recommend using the *orient-mat-based* method as a best practice for measuring hand joint rotation angles with action cameras and ArUco markers.

Acknowledgment

An early version of this paper is published in the ASME IDETC/CIE 2021 conference. The work of Tianyun Yuan is funded by the program of China Scholarship Council (No. 201706120017).

Conflict of Interest

There are no conflicts of interest.

References

[1] ASSH, 2021, "Body Anatomy: Upper Extremity Joints | The Hand Society," https://www.assh.org/handcareprod/safety/joints, Accessed June 15, 2021.
[2] Bullock, I. M., Júlia, B., and Aaron, M. D., 2012, "Assessing Assumptions in Kinematic Hand Models: A Review," 4th IEEE RAS & EMBS International Conference on Biomedical Robotics and Biomechatronics (BioRob), Rome, Italy, June 24–27, pp. 139–146.
[3] Kuch, J. J., and Huang, T. S., 1994, "Human Computer Interaction via the Human Hand: A Hand Model," Proceedings of 1994 28th Asilomar Conference on Signals, Systems and Computers, Pacific Grove, CA, Oct. 31–Nov. 2, pp. 1252–1256.
[4] Reissner, L., Gabriella, F., Renate, L., Pietro, G., and Maurizio, C., 2019, "Assessment of Hand Function During Activities of Daily Living Using Motion Tracking Cameras: A Systematic Review," Proc. Inst. Mech. Eng. Part H: J. Eng. Med., **233**(8), pp. 764–783.
[5] Yang, Y., Yuan, T., Huysmans, T., Elkhuizen, W. S., Tajdari, F., and Song, Y., 2021, "Posture-Invariant Three Dimensional Human Hand Statistical Shape Model," ASME J. Comput. Inf. Sci. Eng., **21**(3), p. 031006.
[6] Yang, Y., Xu, J., Elkhuizen, W. S., and Song, Y., 2021, "The Development of a Low-Cost Photogrammetry-Based 3D Hand Scanner," HardwareX, **10**, p. e00212.
[7] Buckingham, G., 2021, "Hand Tracking for Immersive Virtual Reality: Opportunities and Challenges," arXiv preprint, Accessed November 15, 2021.
[8] Hsiao, J. H., Deng, Y. H., Pao, T. Y., Chou, H. R., and Chang, J. Y., 2017, "Design of a Wireless 3d Hand Motion Tracking and Gesture Recognition Glove for Virtual Reality Applications," Proceedings of ISPS, San Francisco, CA, Aug. 29–30, ASME Paper No. ISPS2017-5450.
[9] Thakur, A., and Rai, R., "User Study of Hand Gestures for Gesture Based 3D CAD Modeling," Proceedings of IDETC/CIE, Boston, MA, Aug. 2–5, ASME Paper No. DETC2015-46086.
[10] Bullock, I. M., Ma, R. R., and Dollar, A. M., 2013, "A Hand-Centric Classification of Human and Robot Dexterous Manipulation," IEEE Trans. Haptics, **6**(2), pp. 129–144.
[11] Wang, J., Barry, O., Kurdila, A. J., and Vijayan, S., "On the Dynamics and Control of a Full Wrist Exoskeleton for Tremor Alleviation," Dynamic Systems and Control Conference, Part City, UT, Oct. 8–11.
[12] Ten Kate, J., Smit, G., and Breedveld, P., 2017, "3D-Printed Upper Limb Prostheses: A Review," Disabil. Rehabil. Assist. Technol., **12**(3), pp. 300–314.
[13] Hamilton, G. F., and Lachenbruch, P. A., 1969, "Reliability of Goniometers in Assessing Finger Joint Angle," Phys. Ther., **49**(5), pp. 465–469.
[14] Reissner, L., Fischer, G., List, R., Taylor, W. R., Giovanoli, P., and Calcagni, M., 2019, "Minimal Detectable Difference of the Finger and Wrist Range of Motion: Comparison of Goniometry and 3D Motion Analysis," J. Orthop. Surg. Res., **14**(1), pp. 1–10.
[15] Ellis, B., and Bruton, A., 2002, "A Study to Compare the Reliability of Composite Finger Flexion With Goniometry for Measurement of Range of Motion in the Hand," Clin. Rehabil., **16**(5), pp. 562–570.
[16] Lewis, E., Fors, L., and Tharion, W. J., 2010, "Interrater and Intrarater Reliability of Finger Goniometric Measurements," Am. J. Occup. Ther., **64**(4), pp. 555–561.
[17] Erol, A., Bebis, G., Nicolescu, M., Boyle, R. D., and Twombly, X., 2007, "Vision-Based Hand Pose Estimation: A Review," Comput. Vis. Image Understand., **108**(1–2), pp. 52–73.
[18] Zhou, H., and Hu, H., 2008, "Human Motion Tracking for Rehabilitation—A Survey," Biomed. Signal Process. Control, **3**(1), pp. 1–18.
[19] Chen, W., Yu, C., Tu, C., Lyu, Z., Tang, J., Ou, S., Fu, Y., and Xue, Z., 2020, "A Survey on Hand Pose Estimation With Wearable Sensors and Computer-Vision-Based Methods," Sensors, **20**(4), p. 1074.
[20] Yang, H., Shao, L., Zheng, F., Wang, L., and Song, Z., 2011, "Recent Advances and Trends in Visual Tracking: A Review," Neurocomputing, **74**(18), pp. 3823–3831.
[21] Connolly, J., Condell, J., O'Flynn, B., Sanchez, J. T., and Gardiner, P., 2017, "IMU Sensor-Based Electronic Goniometric Glove for Clinical Finger Movement Analysis," IEEE Sens. J., **18**(3), pp. 1273–1281.
[22] Salchow-Hömmen, C., Callies, L., Laidig, D., Valtin, M., Schauer, T., and Seel, T., 2019, "A Tangible Solution for Hand Motion Tracking in Clinical Applications," Sensors, **19**(1), p. 208.
[23] Lin, B. S., Lee, I., Yang, S. Y., Lo, Y. C., Lee, J., and Chen, J. L., 2018, "Design of an Inertial-Sensor-Based Data Glove for Hand Function Evaluation," Sensors, **18**(5), p. 1545.
[24] Baldi, T. L., Mohammadi, M., Scheggi, S., and Prattichizzo, D., 2015, "Using Inertial and Magnetic Sensors for Hand Tracking and Rendering in Wearable Haptics," Proceedings of IEEE World Haptics Conference (WHC), IL, June 22–26, pp. 381–387.
[25] NDI, "3D Guidance Sensors—NDI," https://www.ndigital.com/products/3d-guidance/3d-guidance-sensors/, Accessed August 10, 2021.
[26] Saggio, G., Riillo, F., Sbernini, L., and Quitadamo, L. R., 2015, "Resistive Flex Sensors: A Survey," Smart Mater. Struct., **25**(1), p. 013001.
[27] Michaud, H. O., Dejace, L., De Mulatier, S., and Lacour, S. P., "Design and Functional Evaluation of an Epidermal Strain Sensing System for Hand Tracking," Proceedings of IEEE/RSJ International Conference on Intelligent Robots and Systems (IROS), Daejeon, South Korea, Oct. 9–14, pp. 3186–3191.
[28] CyberGlove Systems LLC, "CyberGlove III—CyberGlove Systems LLC," http://www.cyberglovesystems.com/cyberglove-iii/, Accessed August 10, 2021.
[29] Jarque-Bou, N. J., Atzori, M., and Müller, H., 2020, "A Large Calibrated Database of Hand Movements and Grasps Kinematics," Sci. Data, **7**(1), pp. 1–10.
[30] Fischer, G., Jermann, D., List, R., Reissner, L., and Calcagni, M., 2020, "Development and Application of a Motion Analysis Protocol for the Kinematic Evaluation of Basic and Functional Hand and Finger Movements Using Motion Capture in a Clinical Setting—A Repeatability Study," Appl. Sci., **10**(18), p. 6436.

[31] Coupier, J., Hamoudi, S., Telese-Izzi, S., Feipel, V., Rooze, M., and Jan, S. V. S., 2016, "A Novel Method for In-Vivo Evaluation of Finger Kinematics Including Definition of Healthy Motion Patterns," Clin. Biomech., **31**, pp. 47–58.
[32] Garrido-Jurado, S., Muñoz-Salinas, R., Madrid-Cuevas, F. J., and Marín-Jiménez, M. J., 2014, "Automatic Generation and Detection of Highly Reliable Fiducial Markers Under Occlusion," Pattern Recognit., **47**(6), pp. 2280–2292.
[33] Elangovan, N., Dwivedi, A., Gerez, L., Chang, C. M., and Liarokapis, M., 2019, "Employing imu and Aruco Marker Based Tracking to Decode the Contact Forces Exerted by Adaptive Hands," Proceedings of IEEE-RAS 19th International Conference on Humanoid Robots (Humanoids), Toronto, Canada, Oct. 15–17, pp. 525–530.
[34] Mueller, F., Bernard, F., Sotnychenko, O., Mehta, D., Sridhar, S., Casas, D., and Theobalt, C., 2018, "Ganerated Hands for Real-Time 3d Hand Tracking From Monocular rgb," Proceedings of the IEEE Conference on Computer Vision and Pattern Recognition, Salt Lake City, UT, June 18–23, pp. 49–59.
[35] Yuan, S., Ye, Q., Stenger, B., Jain, S., and Kim, T. K., 2017, "Bighand2. 2m Benchmark: Hand Pose Dataset and State of the art Analysis," Proceedings of the IEEE Conference on Computer Vision and Pattern Recognition., Honolulu, HI, July 21–26, pp. 4866–4874.
[36] Garcia-Hernando, G., Yuan, S., Baek, S., and Kim, T. K., 2018, "First-Person Hand Action Benchmark With rgb-d Videos and 3d Hand Pose Annotations," Proceedings of the IEEE Conference on Computer Vision and Pattern Recognition, Salt Lake City, UT, June 18–23, pp. 409–419.
[37] Huysmans, T., and Molenbroek, J. F. M., "DINED/Anthropometry in Design," https://dined.io.tudelft.nl/en, Accessed August 10, 2021.
[38] Oberkampf, D., DeMenthon, D. F., and Davis, L. S., 1996, "Iterative Pose Estimation Using Coplanar Feature Points," Comput. Vis. Image Understand., **63**(3), pp. 495–511.
[39] Cooney, W. P., III, and Chao, E. Y., 1977, "Biomechanical Analysis of Static Forces in the Thumb During Hand Function," J. Bone Jt. Surg. American Volume, **59**(1), pp. 27–36.
[40] Chao, E. Y. S., An, K.-N., Cooney, W. P., and Linscheid, R. L., 1989, *Biomechanics of the Hand*, Y. S. Cappo, ed., World Scientific, Singapore, pp. 73–96.
[41] Wu, G., Van der Helm, F. C., Veeger, H. D., Makhsous, M., Van Roy, P., Anglin, C., Nagels, J., et al., 2005, "ISB Recommendation on Definitions of Joint Coordinate Systems of Various Joints for the Reporting of Human Joint Motion—Part II: Shoulder, Elbow, Wrist and Hand," J. Biomech., **38**(5), pp. 981–992.
[42] McGinley, J. L., Baker, R., Wolfe, R., and Morris, M. E., 2009, "The Reliability of Three-Dimensional Kinematic Gait Measurements: A Systematic Review," Gait Posture, **29**(3), pp. 360–369.
[43] Cheng, P. L., and Pearcy, M., 1999, "A Three-Dimensional Definition for the Flexion/Extension and Abduction/Adduction Angles," Med. Biol. Eng. Comput., **37**(4), pp. 440–444.
[44] Bain, G. I., Polites, N., Higgs, B. G., Heptinstall, R. J., and McGrath, A. M., 2015, "The Functional Range of Motion of the Finger Joints," J. Hand Surg. (European Volume), **40**(4), pp. 406–411.
[45] Mueller, F., Mehta, D., Sotnychenko, O., Sridhar, S., Casas, D., and Theobalt, C., 2017, "Real-Time Hand Tracking Under Occlusion From an Egocentric rgb-d Sensor," Proceedings of the IEEE International Conference on Computer Vision, Venice, Italy, Oct. 22–29, pp. 1154–1163.